Plasmonic Nanoparticle Networks for Light and Heat Concentration

Audrey Sanchot,[†] Guillaume Baffou,[‡,⊥] Renaud Marty,[†] Arnaud Arbouet,[†] Romain Quidant,[‡,§,*] Christian Girard,[†] and Erik Dujardin[†,*]

[†]CEMES, UPR 8011, CNRS-Université de Toulouse, 29 Rue Jeanne Marvig, BP 94347, F-31055 Toulouse, France, [‡]ICFO, Institut de Ciencies Fotoniques, Mediterranean Technology Park, 08860, Castelldefels (Barcelona), Spain, and [§]ICREA, Institucio Catalana de Recerca i Estudis Avancats, 08010 Barcelona, Spain. [⊥]Present address: Institut Fresnel, CNRS, Aix-Marseille Universite, Ecole Centrale de Marseille, Domaine Universitaire Saint-Jerome, F-13397 Marseille, France.

ABSTRACT

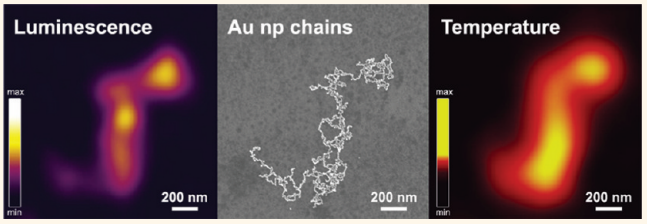

Self-assembled plasmonic nanoparticle networks (PNN) composed of chains of 12 nm diameter crystalline gold nanoparticles exhibit a longitudinally coupled plasmon mode centered at 700 nm. We have exploited this longitudinal absorption band to efficiently confine light fields and concentrate heat sources in the close vicinity of these plasmonic chain networks. The mapping of the two phenomena on the same superstructures was performed by combining two-photon luminescence and fluorescence polarization anisotropy imaging techniques. Besides the light and heat concentration, we show experimentally that the planar spatial distribution of optical field intensity can be simply modulated by controlling the linear polarization of the incident optical excitation. On the contrary, the heat production, which is obtained here by exciting the structures within the optically transparent window of biological tissues, is evenly spread over the entire PNN. This contrasts with the usual case of localized heating in continuous nanowires, thus opening opportunities for these networks in light-induced hyperthermia applications. Furthermore, we propose a unified theoretical framework to account for both the nonlinear optical and thermal near-fields around PNN. The associated numerical simulations, based on a Green's function formalism, are in excellent agreement with the experimental images. This formalism therefore provides a versatile tool for the accurate engineering of optical and thermodynamical properties of complex plasmonic colloidal architectures.

KEYWORDS: self-assembled plasmonics · two-photon luminescence · light-induced heating · gold nanoparticles

The optical properties of suspensions of individual colloidal metal nanoparticles have been scrutinized for more than a century, yet the rational design of their spectral properties by the tailoring of their size and shape has become a topic of interest only recently.[1] In the general context of plasmon-based technology, the next challenge for nanoparticle-based plasmonics is the control of the coupling between localized surface plasmons (LSP) by mastering the spatial organization of nanoparticles.[2−4] Self-assembly and templating principles have been proposed as the most adequate approaches to promote interparticle coupling and ordered multiscale organization toward the design of specific nano-optical functionalities.

In this context, we have recently reported the simple fabrication of complex and extended networks of interconnected chains of gold nanoparticles by a spontaneous one-pot self-assembly process driven by interparticle dipolar interactions.[3,5,6] In suspension, these superstructures exhibit an overall globular size of typically 2−3 μm, but individual chain segments are one-nanoparticle, *i.e.*, 12 nm, wide. As illustrated in Figure 1, the optical absorption spectra of these superstructures, which we call plasmonic nanoparticle networks (PNN), display not only a transverse plasmon mode (520 nm) but also a lower energy mode (700 nm) resulting from the strong coupling of nanoparticle surface plasmons between neighboring nanoparticles along the chains and that we therefore called the PNN longitudinal mode.[7,8]

More recently, suspended PNN were deposited as intact and well-spread networks by developing a specific substrate surface chemistry in order to control deposition and drying regime of the liquid colloidal solution.[9]

The combination of the micrometer-scale size of particle assembly and the 12 nm feature size of individual colloidal constituents confers to these self-assembled architectures the unique ability to modulate very finely the spatial distribution of the electromagnetic field intensity. Once brought onto a solid surface, these colloidal superstructures could contribute to the improvement of applications as diverse as sensors, optical

* Address correspondence to romain.quidant@icfo.es, erik.dujardin@cemes.fr.

Received for review February 1, 2012 and accepted March 6, 2012.

Published online March 06, 2012
10.1021/nn300470j

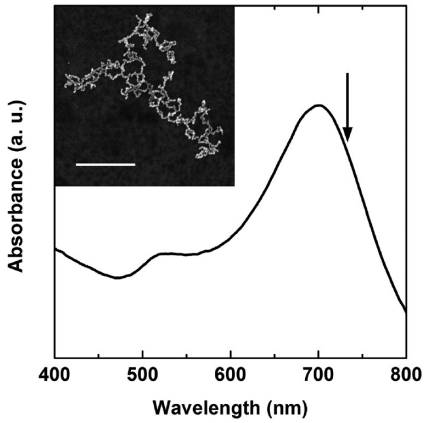

Figure 1. Typical extinction spectrum of plasmonic nanoparticle networks (PNN) revealing both transversal (520 nm) and longitudinal (700 nm) absorption bands. The arrow indicates the laser excitation of the longitudinal absorption band in our experiments. Inset: SEM image of a PNN. Scale bar: 500 nm.

interconnects, enhanced nanoscale spectroscopy, and microscopy.

Concomitantly, the optical characterization down to subwavelength and molecular-scale features has made significant progress with the recent development of near-field[7,10−12] and single-molecule microscopy,[13,14] electron energy loss spectroscopy (EELS) and imaging,[15] or even suitable far- field microscopy methods.[16−20] In particular, two-photon luminescence (TPL) has been implemented in both near-field[11,12] and far-field[21−23] configurations. In the latter case, the TPL intensity can be related, in a first approximation, to the square of the field intensity in the metal, *i.e.*, the fourth power of the local electric field.[23] With such a fast-varying spatial dependency, far-field TPL microscopy reaches a spatial resolution as high as 200 nm.[24] Interestingly, optically induced dissipation in plasmonic structures has also been characterized locally by far-field microscopy techniques such as fluorescence polarization anisotropy (FPA) imaging.[24] This indirect temperature measurement consists in measuring the loss of fluorescence anisotropy of a molecular probe in solution, upon linearly polarized excitation, when it crosses regions of elevated temperature due to heat dissipation in the vicinity of the illuminated plasmonic structure. When the entire plasmonic structure is illuminated while the FPA is probed locally, one measures the temperature distribution as detailed in refs 25 and 26. On the contrary, when the illumination of the metal is confocal to the fluorescence excitation, then the FPA signal is related to the local heat source density.[24]

In this article, we report on the experimental observations and numerical simulations of near-field optical intensity and temperature mapping in the vicinity of gold PNN. The large longitudinal band of these networks (Figure 1) is used to excite the coupled

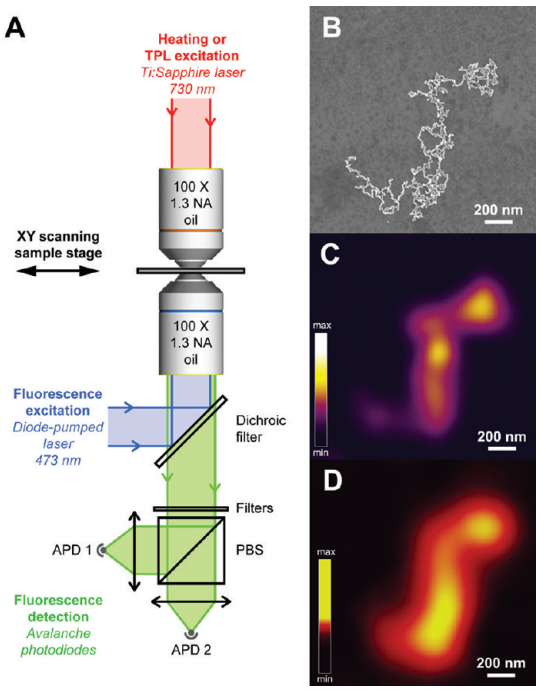

Figure 2. (A) Schematic view of the combined TPL-FPA experimental setup. (B) SEM image of a small PNN deposited on ITO/glass substrate. (C) TPL and (D) Temperature images of the same PNN excited at 730 nm.

modes in the chains around 730 nm with a hybrid microscope combining TPL and FPA measurements.

The investigation of the plasmonic properties of lithographically designed metal structures by this combined technique was first introduced in ref 24, and the experimental setup is illustrated in Figure 2A. PNN are obtained by adding 2-mercaptoethanol (MEA; $HS(CH_2)_2OH$) to Au nanoparticle solutions under conditions detailed elsewhere[3] and summarized in the Experimental Details section.

Freshly prepared PNN are deposited on glass/ITO coverslips.[9] Well-spread networks were identified by FEG-SEM imaging (Figure 2B). The TPL measurements were obtained by tightly focusing on the sample a pulsed IR Ti:Sapphire laser set at 730 nm (see Experimental Details). An image is constructed by raster scanning the sample and collecting the emitted light through a large numerical aperture objective (Figure 2C).

To perform the temperature increase measurements, two laser beams are focused and overlapped.[28] The IR Ti:Sapphire laser locally heats the PNN, while a second linearly polarized blue laser is used to excite the fluorescein molecules dispersed in a glycerol/water mixture surrounding the structure. The emitted molecular fluorescence is collected through the bottom objective and sent to two APDs to construct two fluorescence maps corresponding to two perpendicular emission polarization directions (see Experimental Details). The loss in fluorescence anisotropy is calculated from the polarization difference signal, and the associated temperature map is then obtained by using

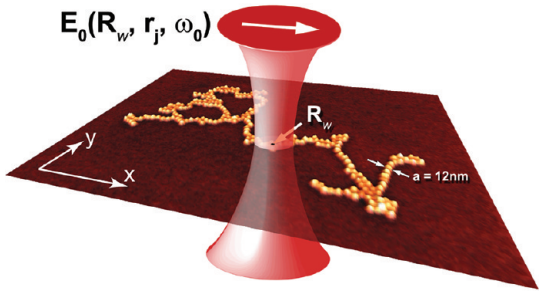

Figure 3. Schematic view of the experimental configuration in which a PNN made of 12 nm diameter nanoparticles is illuminated in normal incidence by a focused laser beam characterized by an electric field vector $E_0(R_w, r, \omega_0)$, R_w, r_i, and ω_0 being the beam waist position, the considered location for E_0, and the incident field pulsation.

a FPA = $f(T)$ calibration curve described elsewhere (Figure 2D).[28] To get the temperature increase as a function of the IR laser location, the sample is raster scanned in X and Y as for the TPL measurements. For both types of experiments, particular care was taken to strictly avoid any damage of the nanoparticles by the laser-induced heating. The onset of melting could easily be identified in TPL by the rapid variation and eventual disappearance of the TPL signal within a few pixels. It usually occurred for a nominal IR laser power of about 10 mW. The IR laser power used in all experiments was kept below 30% of that needed for damaging the nanoparticles.

Finally, the SEM images of the measured samples were resolved enough to extract positional maps of each individual 12 nm diameter nanoparticle from the studied PNN. These experimental maps were used to compute the TPL and temperature maps.

This theoretical analysis was based on a novel numerical tool involving the computation of temperature increase and TPL signal through a complete self-consistent scheme using both electrodynamical and thermal Green functions.[29] In the following, our model is first described in detail, and both experimental TPL and FPA images are then compared to simulated ones for one in several studied PNN.

At the nanometer scale, the optical properties of small plasmonic objects deposited on a surface (small individual or self-assembled colloidal particles) can be investigated by adapting the coupled dipole approximation method[30] to a planar geometry.[7] We first describe the unified formalism and numerical method that we developed in this context to compute the TPL and temperature distributions near PNNs, as depicted in Figure 3. The network is composed of N identical subwavelength-sized nanoparticles (12 nm) located at the positions r_i. When the sample is illuminated by the electric field $\mathbf{E}_0(\mathbf{R}_w, \mathbf{r}, \omega_0)$ associated with a monochromatic laser beam of frequency ω_0 centered and focused at $\mathbf{R}_w$, each nanometric component acquires an oscillating dipole moment driven by the local electric field $\mathbf{E}(\mathbf{R}_w, \mathbf{r}_i, \omega_0)$, which originates from the many-body interactions with the other particles:

$$\mathbf{P}(\mathbf{R}_w, \mathbf{r}_i, \omega_0) = \alpha(\omega_0) \cdot \mathbf{E}(\mathbf{R}_w, \mathbf{r}_i, \omega_0) \quad (1)$$

where $\alpha(\omega_0)$ characterizes the dipolar polarizability of the metal particles. The many-body interactions between the nanoparticles can be introduced by writing N implicit linear equations:

$$\mathbf{E}(\mathbf{R}_w, \mathbf{r}_i, \omega_0) = \mathbf{E}_0(\mathbf{R}_w, \mathbf{r}_i, \omega_0) + \sum_j \mathbf{S}(\mathbf{r}_i, \mathbf{r}_j, \omega_0) \cdot \alpha(\omega_0) \cdot \mathbf{E}(\mathbf{R}_w, \mathbf{r}_j, \omega_0) \quad (2)$$

where $\mathbf{S}(\mathbf{r}_i, \mathbf{r}_j, \omega_0)$ represents the Green dyadic function of the bare substrate.[7]

The TPL signal arising from the gold nanoparticles is a noncoherent process characterized by a wide spectrum spanning from ω_0 to $2\omega_0$. This process is related to the intensity distribution $|\mathbf{E}(\mathbf{R}_w, \mathbf{r}_i, \omega_0)|^2$ of local electric fields experienced by each particle. To solve this problem, we assume that the TPL signal can be modeled by summing the different intensities $|\mathbf{E}(\mathbf{R}_w, \mathbf{r}_i, \omega_0)|^2$ rather than the electric field amplitudes $\mathbf{E}(\mathbf{R}_w, \mathbf{r}_i, \omega_0)$ to account for the noncoherent nature of the TPL process:

$$I_{\mathrm{TPL}}(\mathbf{R}_w, \omega_0) \propto [\sum_{i=1}^{N} |\mathbf{E}_i(\mathbf{R}_w, \omega_0)|^2]^2 \quad (3)$$

The overall square is intended to account for the two-photon absorption.

In Figure 4, we present a sequence of theoretical (Figure 4A,B) and experimental (Figure 4C,D) TPL images obtained by scanning the tightly focused Ti:Sapphire laser spot with respect to a PNN composed of 1537 gold nanoparticles, the SEM image of which can be seen in the background of panels C and D. For each position of the laser beam waist $\mathbf{R}_w$ (incident wavelength λ_0 = 730 nm), the simulated TPL intensity has been computed from the equation (3) by introducing the coordinates of the gold particle map plotted as an overlay in black circles in panels A and B into the numerical code. The two incident polarizations, investigated along the OX and OY directions, show an excellent agreement between experimental data and simulations, indicating that TPL measurements provide quantitative information on the light confinement near extremely small gold structures. Although the TPL signal seems to be more intense in regions of denser particle packing, this correlation does not account for the observed polarization dependency of the images. This polarization effect suggests that the local anisotropy of uniaxially coupled nanoparticles translates into anisotropic light confinement upon excitation of the PNN at 730 nm.

Although limited by the intrinsic sensitivity and spatial resolution of our microscopy setup, these observations illustrate how strongly coupled nanoparticles of small size but high crystallinity are able to

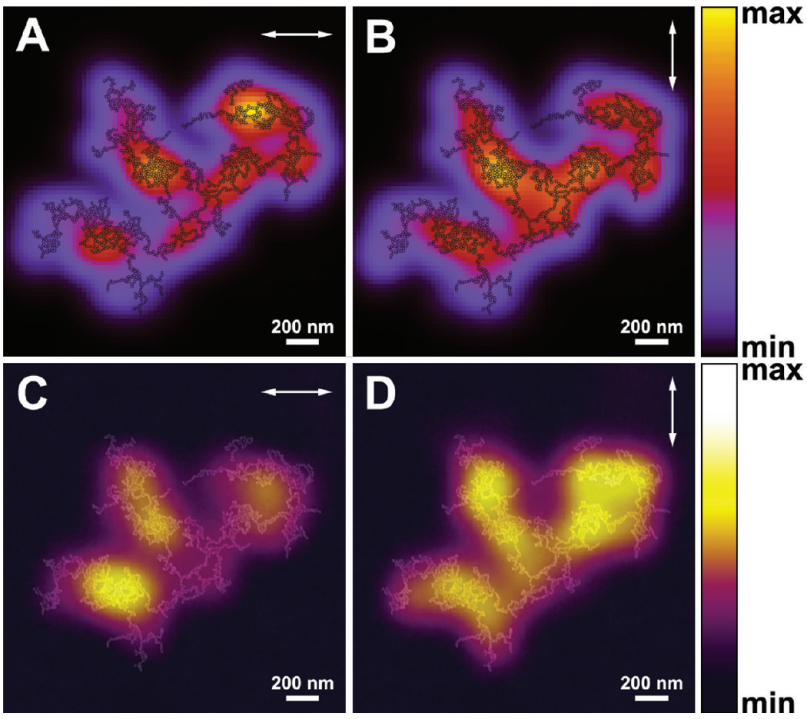

Figure 4. TPL mapping near a large PNN composed of 1537 gold nanoparticles (image size 2 × 2 μm). (A, B) Simulation images obtained from eq 3 overlaid with the nanoparticle map. (C, D) Experimental TPL images measured on this PNN overlaid with the SEM image of the PNN. Incident polarization is aligned along OX for (A) and (C) and along OY for (B) and (D).

laterally confine the electromagnetic intensity within a few tens of nanometers, while allowing its distribution along chains of a few hundreds of nanometers, as demonstrated theoretically elsewhere.[7]

Simultaneously, during the IR illumination, the PNN temperature rises because of the Joule effect induced inside the metal particles. The heat power Q_i delivered by each nanoparticle can be computed from the electric field amplitude $\mathbf{E}_i(\mathbf{R}_w, \omega_0)$ using the relation[24]

$$Q_i(\mathbf{R}_w, \omega_0) = \frac{\omega_0 \mathrm{Im}[\alpha(\omega_0)]}{2} |\mathbf{E}_i(\mathbf{R}_w, \omega_0)|^2 \qquad (4)$$

From this relation, the temperature rise, $\Delta T(\mathbf{R}_w, \omega_0)$, expected at the laser location $\mathbf{R}_w$ can be deduced using the thermal Green's function:[29]

$$\Delta T(\mathbf{R}_w, \omega_0) = \frac{1}{4\pi\kappa} \sum_{i=1}^{N} \frac{Q_i(\mathbf{R}_w, \omega_0)}{|\mathbf{R}_w - \mathbf{r}_i|} \qquad (5)$$

where κ is the thermal conductivity of the surroundings. In order to take into account the influence of the substrate conductivity, the image method has been used to compute the temperature distribution induced by the PNNs.[29]

Figure 5 shows a sequence of temperature maps resulting from the scanning of the same large PNN described in Figure 4 through a 300 nm confocal spot of the near-IR and blue lasers .

Although much less confined than the optical near-field intensity revealed in the TPL maps of Figure 4, the temperature distribution faithfully reproduces the PNN morphology. Noticeably, these thermal maps do not display any significant variation with the incident polarization (see maps 5C and 5D). In particular, the three main branches of the network generate the same temperature rise because they are composed of many linear chains able to support the excited longitudinal mode irrespectively of the incident polarization. In addition, although we deal with extremely localized heat sources, the temperature distribution appears smoother than the near-field optical intensity map induced near the same system because of the thermal diffusion.[31] Two key differences between the generation of heat and optical TPL intensity should be emphasized. In the first case, as illustrated by eq 5, the temperature distribution generated at location $\mathbf{R}_{obs}$ by a point-like heat source located at $\mathbf{R}_h$ varies like the inverse of $|\mathbf{R}_{obs} - \mathbf{R}_h|$, while it varies like the inverse of the third power of this distance in the case of the optical near-field.

Furthermore, the TPL signal is sensitive to the square of the optical near-field intensity (*cf.* eq 3), while the thermal process is just proportional to the global near-field intensity (*cf.* eq 5). This is clearly illustrated in both experimental and theoretical images of Figure 4, where we observe a significant variation of the TPL pattern inside the three branches of the PNN when the polarization is rotated by 90°, in contrast to the invariance of thermal maps in Figure 5.

Interestingly, the excitation of longitudinally coupled modes in PNN involves electrically separated

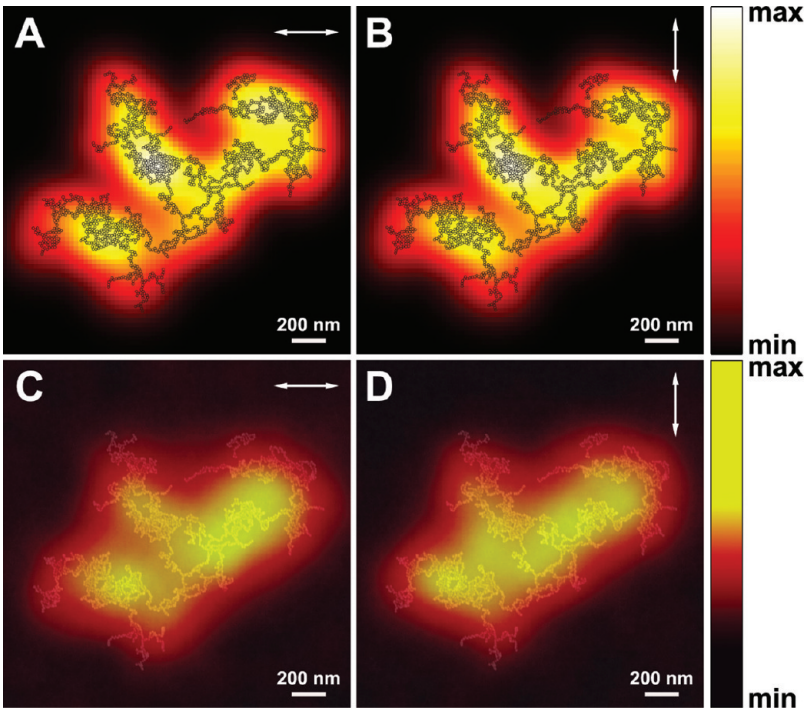

Figure 5. Temperature mapping near the same large PNN shown in Figure 4. (A, B) Simulation images obtained from eq 5. (C, D) Experimental images measured by the fluorescence polarization anisotropy of fluorescein molecules surrounding the PNN. Incident polarization is aligned along OX for (A) and (C) and along OY for (B) and (D). Calculated (A, B) and experimental (C, D) images are respectively overlaid with the positional network particle map and the SEM image of the PNN.

nanoparticles in contrast to the continuous metallic stripes or nanowires prepared by lithographic approaches[24] or colloidal synthesis. As a consequence, the energy dissipation originates from each individual nanoparticle and is homogeneously distributed along the nanoparticle chains rather than localized where the excited nanorod plasmon mode induces a maximal current, as shown in ref 24. The self-assembly of the nanoparticles into globular micrometer-scale PNN therefore combines a number of specificities that could be advantageously exploited in the context of hyperthermia cell treatment.[32] Although the full assessment of the hyperthermia efficiency of PNN on live bacteria, which is currently underway, lies beyond the scope of this article, the assets of our system already appear in the present results. Indeed, the heat production in PNN is obtained by addressing the longitudinally coupled mode centered at 700 nm that allows an excitation through the transparency window of biological tissues. Moreover, by choosing this wavelength, no individual stray particles or particle short chains (less than 4 or 5 nanoparticles) are excited, therefore obviating the parasitic heat dissipation away from the PNN. Moreover, the commensurability of the PNN with cell size, the biocompatibility of gold nanoparticles, and the spontaneous affinity of PNN for the cell membrane (Figure S1 in the Supporting Information) strongly suggest that optical energy could be dissipated directly at the PNN-wrapped cell walls without requiring an internalization step.

CONCLUSION

In conclusion, this work demonstrates for the first time that large colloidal microstructures made of 12 nm diameter, crystalline nanoparticles self-assembled into single particle chains are able to effectively modulate the 2D spatial distribution of electromagnetic intensity, once deposited onto a substrate. Since the self-assembled networks are excited in the longitudinal coupled mode borne by the chains, these energy distributions can be simply tuned by changing the polarization of the incident light. The investigation of the near-field using TPL mapping provides an efficient means to characterize the intensity distribution at the scale of the entire superstructure but also reveals in-plane field modulation features that are limited only by the intrinsic spatial resolution of our TPL setup, namely *ca.* 200 nm. Therefore, PNN are shown to have a unique potential for confining and enhancing the electromagnetic field down to sub-100 nm length scale.

Moreover, the measurement of the temperature distribution with our dual setup has shown that heat is efficiently generated by exciting the longitudinal coupled mode, and the generated heat is confined near the PNN. Understandably, the spatial distribution of the temperature elevation is more homogeneous and less sensitive to incident polarization than the TPL signal. Nevertheless, the optically induced localized heat dissipation in our water-dispersible gold

nanoparticle self-assembly holds promises in biomedical applications beyond the current capabilities of individual colloids or substrate-bound metal structures.

Finally, we have developed a model and simulation tool that accounts for most of the observed 2D field map features. This is now a useful tool for the engineering of the optical near-field, for example for nanoscale optical information processing devices, using self-assembled structures made of crystalline metal colloids. The extension of our model and simulation tool to dissipation phenomena faithfully reproduced the observed temperature maps.

EXPERIMENTAL DETAILS

Au Nanoparticle Synthesis and PNN Self-Assembly. Isometric gold nanoparticles were freshly prepared by the citrate reduction method[27] at a citrate:$[AuCl_4]^-$ molar ratio of 5.2:1 and diluted to the required concentration with 18 MΩ deionized water. The average diameter of the Au nanoparticles used in all experiments was 11.8 ± 1.1 nm. The assembly of the PNN was performed at room temperature by adding 2-mercaptoethanol ($HS(CH_2)_2OH$) to Au nanoparticle solutions at a Au nanoparticle:MEA molar ratio of 1:5000. The nanoparticle chain assembly is characterized by a color change from pink to purple as the coupled modes emerge. It was monitored by UV−vis spectrophotometry. The assembly is complete within 24 to 48 h after mixing.

TPL and FPA Sample Preparation. Freshly prepared PNN are deposited on cleaned glass coverslips coated with a 10 nm conductive indium tin oxide (ITO) layer and imaged by FEG-SEM on a Zeiss 1540XB Gemini column.

TPL Measurements. For TPL experiments, an IR Ti:Sapphire laser operated in pulsed mode is tightly focused on the sample with a high numerical aperture objective (NA = 1.3). The typical IR laser power is 1−3 mW, and the pulse duration is 180 fs. In all the experiments, the IR laser wavelength was set to 730 nm. An image is obtained by raster scanning the sample in X and Y using a piezo stage and collecting the emitted light on an avalanche photodiode through another NA = 1.3 objective.

FPA Measurements. For FPA experiments, two laser beams are focused and overlapped. The IR Ti:Sapphire laser is set in cw mode, while a second linearly polarized blue laser is used to excite the fluorescein molecules dispersed in a glycerol/water mixture surrounding the structure. The typical power of the blue and IR lasers is 60 μW and 4 mW, respectively. The emitted molecular fluorescence is collected through the bottom objective onto two APDs *via* a polarizing cubic beam splitter. The loss in fluorescence anisotropy is calculated from the polarization difference signal. To get the temperature increase as a function of the IR laser location, the sample is raster scanned in X and Y as for the TPL measurements.

Conflict of Interest: The authors declare no competing financial interest.

Acknowledgment. This work was supported by the European Research Council (ERC) (Grant ERC-2007-StG Nr 203872 COMOSYEL to E.D.), the French Agence Nationale de la Recherche (Grant ANR-08-NANO-054-01-NAPHO to C.G. and NT09-451197-PlasTips to E.D.), the French Ministry of Research (Ph.D. fellowships to A.S. and R.M.), and the massively parallel computing center CALMIP in Toulouse. R.Q. also acknowledges the financial support from Fundacio Privada CELLEX and the European Commission's Seventh Framework Programme under Grants SPEDOC (248835) and ERC-Plasmolight (259196). A.S. and E.D. thank M. Li and S. Mann (University of Bristol, UK) for fruitful discussions.

Supporting Information Available: SEM images of bacteria colony and isolated individuals coated with PNN. This material is available free of charge *via* the Internet at http://pubs.acs.org/.

REFERENCES AND NOTES

1. Tao, A. R.; Habas, S.; Yang, P. Shape Control of Colloidal Metal Nanocrystals. *Small* **2008**, *4*, 310–325.
2. Kinge, S.; Crego-Calama, M.; Reinhoudt, D. N. Self-Assembling Nanoparticles at Surfaces and Interfaces. *ChemPhysChem* **2008**, *9*, 20–42.
3. Lin, S.; Li, M.; Dujardin, E.; Girard, C.; Mann, S. One-Dimensional Plasmon Coupling by Facile Self-Assembly of Gold Nanoparticles into Branched Chain Networks. *Adv. Mater.* **2005**, *17*, 2553–2559.
4. Zhang, H.; Edwards, E. W.; Wang, D.; Mohwald, H. Directing the Self-Assembly of Nanocrystals Beyond Colloidal Crystallization. *Phys. Chem. Chem. Phys.* **2006**, *8*, 3288–3299.
5. Zhang, H.; Fung, K.-H.; Hartmann, J.; Chan, C. T.; Wang, D. Controlled Chainlike Agglomeration of Charged Gold Nanoparticles via a Deliberate Interaction Balance. *J. Phys. Chem. C* **2008**, *112*, 16830–16839.
6. Sardar, R.; Shumaker-Parry, J. S. Asymmetrically Functionalized Gold Nanoparticles Organized in One-Dimensional Chains. *Nano Lett.* **2008**, *8*, 731–736.
7. Girard, C.; Dujardin, E.; Li, M.; Mann, S. Theoretical Near-Field Optical Properties of Branched Plasmonic Nanoparticle Networks. *Phys. Rev. Lett.* **2006**, *97*, 100801.
8. Girard, C.; Dujardin, E. Near-Field Optical Properties of Top-Down and Bottom-Up Nanostructures. *J. Opt. A: Pure Appl. Opt.* **2006**, *8*, S73.
9. Bonell, F.; Sanchot, A.; Dujardin, E.; Pechou, R.; Girard, C.; Li, M.; Mann, S. Processing and Near-Field Optical Properties of Self-Assembled Plasmonic Nanoparticle Networks. *J. Chem. Phys.* **2009**, *130*, 034702.
10. Dickson, R. M.; Lyon, L. A. Unidirectional Plasmon Propagation in Metallic Nanowires. *J. Phys. Chem. B* **2000**, *104*, 6095–6098.
11. Imura, K.; Nagahara, T.; Okamoto, H. Imaging of Surface Plasmon and Ultrafast Dynamics in Gold Nanorods by Near-Field Microscopy. *J. Phys. Chem. B* **2004**, *108*, 16344–16347.
12. Imura, K.; Nagahara, T.; Okamoto, H. Characteristic Near-Field Spectra of Single Gold Nanoparticles. *Chem. Phys. Lett.* **2004**, *400*, 500–505.
13. Gerton, J. M.; Wade, L. A.; Lessard, G. A.; Ma, Z.; Quake, S. R. Tip-Enhanced Fluorescence Microscopy at 10 Nanometer Resolution. *Phys. Rev. Lett.* **2004**, *93*, 180801.
14. Frey, H. G.; Witt, S.; Felderer, K.; Guckenberger, R. High-Resolution Imaging of Single Fluorescent Molecules with the Optical Near-Field of a Metal Tip. *Phys. Rev. Lett.* **2004**, *93*, 200801.
15. Nelayah, J.; Kociak, M.; Stephan, O.; Garcia de Abajo, F. J.; Tence, M.; Henrard, L.; Taverna, D.; Pastoriza-Santos, I.; Liz-Marzan, L. M.; Colliex, C. Mapping Surface Plasmons on a Single Metallic Nanoparticle. *Nat. Phys.* **2007**, *3*, 348–353.
16. Arbouet, A.; Christofilos, D.; Del Fatti, N.; Vallee, F.; Huntzinger, J. R.; Arnaud, L.; Billaud, P.; Broyer, M. Direct Measurement of the Single-Metal-Cluster Optical Absorption. *Phys. Rev. Lett.* **2004**, *93*, 127401–4.
17. Betzig, E.; Patterson, G. H.; Sougrat, R.; Lindwasser, O. W.; Olenych, S.; Bonifacino, J. S.; Davidson, M. W.; Lippincott-Schwartz, J.; Hess, H. F. Imaging Intracellular Fluorescent Proteins at Nanometer Resolution. *Science* **2006**, *313*, 1642–1645.
18. Rust, M. J.; Bates, M.; Zhuang, X. Sub-Diffraction-Limit Imaging by Stochastic Optical Reconstruction Microscopy (STORM). *Nat. Methods* **2006**, *3*, 793–796.
19. Gaiduk, A.; Yorulmaz, M.; Ruijgrok, P. V.; Orrit, M. Room-Temperature Detection of a Single Molecule Absorption by Photothermal Contrast. *Science* **2010**, *330*, 353–356.
20. Celebrano, M.; Kukura, P.; Renn, A.; Sandoghdar, V. Single-Molecule Imaging by Optical Absorption. *Nat. Photonics* **2011**, *5*, 95–98.

21. Bouhelier, A.; Beversluis, M. R.; Novotny, L. Characterization of Nanoplasmonic Structures by Locally Excited Photoluminescence. *Appl. Phys. Lett.* **2003**, *83*, 5041–5043.
22. Bouhelier, A.; Bachelot, R.; Lerondel, G.; Kostcheev, S.; Royer, P.; Wiederrecht, G. P. Surface Plasmon Characteristics of Tunable Photoluminescence in Single Gold Nanorods. *Phys. Rev. Lett.* **2005**, *95*, 267405.
23. Ghenuche, P.; Cherukulappurath, S.; Taminiau, T. H.; van Hulst, N. F.; Quidant, R. Spectroscopic Mode Mapping of Resonant Plasmon Nanoantennas. *Phys. Rev. Lett.* **2008**, *101*, 116805.
24. Baffou, G.; Girard, C.; Quidant, R. Mapping Heat Origin in Plasmonic Structures. *Phys. Rev. Lett.* **2010**, *104*, 136805.
25. Baffou, G.; Quidant, R.; Girard, C. Heat Generation in Plasmonic Nanostructures: Influence of Morphology. *Appl. Phys. Lett.* **2009**, *94*, 153109.
26. Baffou, G.; Quidant, R.; de Abajo, F. J. G. Nanoscale Control of Optical Heating in Complex Plasmonic Systems. *ACS Nano* **2010**, *4*, 709–716.
27. Frens, G. Controlled Nucleation for the Regulation of the Particle Size in Monodisperse Gold Suspensions. *Nat. Phys. Sci.* **1973**, *241*, 20–22.
28. Baffou, G.; Kreuzer, M. P.; Kulzer, F.; Quidant, R. Temperature Mapping Near Plasmonic Nanostructures Using Fluorescence Polarization Anisotropy. *Opt. Exp.* **2009**, *17*, 3291–3298.
29. Baffou, G.; Quidant, R.; Girard, C. Thermoplasmonics Modeling: A Green's Function Approach. *Phys. Rev. B* **2010**, *82*, 165424.
30. Draine, B. T.; Flatau, P. J. Discrete-Dipole Approximation For Scattering Calculations. *J. Opt. Soc. Am. A* **1994**, *11*, 1491–1499.
31. Ye, E.; Win, K. Y.; Tan, H. R.; Lin, M.; Teng, C. P.; Mlayah, A.; Han, M.-Y. Plasmonic Gold Nanocrosses with Multidirectional Excitation and Strong Photothermal Effect. *J. Am. Chem. Soc.* **2011**, *133*, 8506–8509.
32. Huang, X.; Jain, P.; El-Sayed, I.; El-Sayed, M. Plasmonic Photothermal Therapy (PPTT) Using Gold Nanoparticles. *Lasers Med. Sci.* **2008**, *23*, 217–228.